(2)

AFGL-TR-89-0091

Ground-Based Measurements of Joule Heating Rates

O. de la Beaujardiere
R. Johnson
V.B. Wickwar

SRI International
333 Ravenswood Avenue
Menlo Park, CA 94025

3 April 1989

Scientific Report No. 1

AIR FORCE GEOPHYSICS LABORATORY
AIR FORCE SYSTEMS COMMAND
UNITED STATES AIR FORCE
HANSCOM AIR FORCE BASE, MASSACHUSETTS 01731-5000

"This Technical report has been reviewed and is approved for publication"

FREDERICK J. RICH
Contract Manager

NELSON C. MAYNARD
Branch Chief

FOR THE COMMANDER

RITA C. SAGALYN
Division Director

This report has been reviewed by the ESD Public Affairs Office (PA) and is releasable to the National Technical Information Service (NTIS).

Qualified requestors may obtain additional copies from the Defense Technical Information Center. All others should apply to the National Technical Information Service.

If your address has changed, or if you wish to be removed from the mailing list, or if the addressee is no longer employed by your organization, please notify AFGL/DAA, Hanscom AFB, MA 01731. This will assist us in maintaining a current mailing list.

Do not return copies of this report unless contractual obligations or notices on a specific document requires that it be returned.

Unclassified
SECURITY CLASSIFICATION OF THIS PAGE

REPORT DOCUMENTATION PAGE

1a. REPORT SECURITY CLASSIFICATION Unclassified	1b. RESTRICTIVE MARKINGS
2a. SECURITY CLASSIFICATION AUTHORITY	3. DISTRIBUTION / AVAILABILITY OF REPORT APPROVED FOR PUBLIC RELEASE; DISTRIBUTION UNLIMITED
2b. DECLASSIFICATION / DOWNGRADING SCHEDULE	
4. PERFORMING ORGANIZATION REPORT NUMBER(S)	5. MONITORING ORGANIZATION REPORT NUMBER(S) AFGL-TR-89-0091
6a. NAME OF PERFORMING ORGANIZATION SRI International 6b. OFFICE SYMBOL (If applicable)	7a. NAME OF MONITORING ORGANIZATION Air Force Geophysics Laboratory
6c. ADDRESS (City, State, and ZIP Code) 333 Ravenswood Avenue Menlo Park, CA 94025	7b. ADDRESS (City, State, and ZIP Code) Hanscom AFB Massachusetts 01731-5000
8a. NAME OF FUNDING / SPONSORING ORGANIZATION 8b. OFFICE SYMBOL (If applicable)	9. PROCUREMENT INSTRUMENT IDENTIFICATION NUMBER F19628-87-K-0006
8c. ADDRESS (City, State, and ZIP Code)	10. SOURCE OF FUNDING NUMBERS

PROGRAM ELEMENT NO.	PROJECT NO.	TASK NO.	WORK UNIT ACCESSION NO.
61102F	2311	G5	BC

11. TITLE (Include Security Classification)
Ground-Based Measurements of Joule Heating Rates

12. PERSONAL AUTHOR(S)
O. de la Beaujardiere, R. Johnson, V.B. Wickwar*

13a. TYPE OF REPORT	13b. TIME COVERED	14. DATE OF REPORT (Year, Month, Day)	15. PAGE COUNT
Scientific No. 1	FROM _____ TO _____	1989 April 3	20

16. SUPPLEMENTARY NOTATION Presented at the Proceedings of the International Conference on Auroral Physics, Cambridge, MA, 1988
* Ctr for Atmospheric & Space Sciences, Utah State University

17. COSATI CODES		
FIELD	GROUP	SUB-GROUP

18. SUBJECT TERMS (Continue on reverse if necessary and identify by block number)
Ionosphere, Ionospheric currents, Joule heating, Neutral winds, Incoherent scatter radar

19. ABSTRACT (Continue on reverse if necessary and identify by block number)

Joule heating in the upper atmosphere is the most important energy dissipation process between the magnetosphere and the ionosphere. In this paper we examine the various terms in the equation that governs Joule heating.

(1) The ionospheric electric field seasonal dependence is examined. It is found that the shape of the ionospheric plasma convection cells, and the latitude of the reversal from sunward to antisunward convection, are seasonally dependent. Statistical averages of the square of the ion velocity show a maximum in fall, and a minimum in summer.

(2) Pedersen conductivities at F region altitudes are examined using Chatanika and Sondrestrom radar data. It is shown that during solar minimum conditions, the F region contributes less than 20% to the total height integrated Pedersen conductivity (Σ_P). In contrast, during solar maximum conditions the contribution to Σ_P from solar produced F-region ionization can be 60%.

(3) The importance of the neutral wind term in Joule heating calculations is illustrated using a specific example. The Joule heating calculated by including the neutral wind term is 2 to 4 times smaller than that calculated without the neutral wind. But the reverse can also be true, as shown during a period when the neutral wind played the role of a dynamo in the ionosphere/magnetosphere current.

20. DISTRIBUTION / AVAILABILITY OF ABSTRACT	21. ABSTRACT SECURITY CLASSIFICATION
☐ UNCLASSIFIED/UNLIMITED ☐ SAME AS RPT. ☐ DTIC USERS	Unclassified

22a. NAME OF RESPONSIBLE INDIVIDUAL	22b. TELEPHONE (Include Area Code)	22c. OFFICE SYMBOL
Frederick Rich		AFGL/PHG

DD FORM 1473, 84 MAR 83 APR edition may be used until exhausted. All other editions are obsolete.

SECURITY CLASSIFICATION OF THIS PAGE
Unclassified

GROUND-BASED MEASUREMENTS OF JOULE HEATING RATES

O. DE LA BEAUJARDIÈRE, R. JOHNSON
Geoscience and Engineering Center, SRI International

V. B. WICKWAR
Center for Atmospheric and Space Sciences, Utah State University

ABSTRACT

Joule heating in the upper atmosphere is the most important energy dissipation process between the magnetosphere and the ionosphere. In this paper we examine the various terms in the equation that governs Joule heating.

(1) The ionospheric electric field seasonal dependence is examined. It is found that the shape of the ionospheric plasma convection cells, and the latitude of the reversal from sunward to antisunward convection, are seasonally dependent. Statistical averages of the square of the ion velocity show a maximum in fall, and a minimum in summer.

(2) Pedersen conductivities at F region altitudes are examined using Chatanika and Sondrestrom radar data. It is shown that during solar minimum conditions, the F region contributes less than 20% to the total height integrated Pedersen conductivity Σ_p. In contrast, during solar maximum conditions the contribution to Σ_p from solar produced F-region ionization can be 60%.

(3) The importance of the neutral wind term in Joule heating calculations is illustrated using a specific example. The Joule heating calculated by including the neutral wind term is 2 to 4 times smaller than that calculated without the neutral wind. But the reverse can also be true, as shown during a period when the neutral wind played the role of a dynamo in the ionosphere/ magnetosphere current.

INTRODUCTION

It is generally accepted that the solar wind energy that reaches the magnetosphere is dissipated by three main processes: (1) injection of particles into the ring current and further dissipation by charge exchange, (2) Joule heating in the ionosphere and thermosphere, and (3) particle precipitation. The energy transfer rate into the ring current is often larger than that of the other two processes. At times, however, the Joule heating rate can be the largest [Baumjohann and Kamide, 1984]. Although particle precipitation in the auroral oval may dissipate energy at a rate comparable to Joule dissipation [Evans et al., 1977; Vickrey et al., 1982], globally, the dissipation by Joule heating is significantly more important than by particle precipitation [Baumjohann and Kamide, 1984]. The effect on the neutral atmosphere of the Joule dissipation has far-reaching

Submitted to the Proceedings of the International Conference on Auroral Physics, Cambridge, 1988.

consequences. Joule dissipation heats the neutral gas and causes upwelling of atomic oxygen which is then transported to lower latitudes. This process changes the global configuration of thermospheric neutral winds [Roble et al., 1977; Prölss, 1980]. As a result, the Joule heating rate is one of the most fundamental parameters needed in studies of the coupling mechanisms between the solar wind and the thermosphere-ionosphere-magnetosphere system.

The height-integrated Joule heating rate, in the reference frame of the neutrals, is governed by the equation

$$Q_J = \int_{h_1}^{h_2} \sigma_P(h)(\mathbf{E} + \mathbf{U} \times \mathbf{B})^2 \, dh \qquad (1)$$

where

σ_P is the Pedersen conductivity

E is the electric field calculated from the ionospheric plasma drift **V** by $\mathbf{E} = -\mathbf{V} \times \mathbf{B}$

U is the neutral wind

B is the magnetic field

h_1 and h_2, the limits of integration, encompass the E and F region altitudes.

Incoherent scatter radars are the only ground-based instruments capable of measuring all the quantities in Equation [1]. They can easily measure the electron density, electric field and neutral wind vectors. They can also measure, although with more difficulty, the ion composition and ion-neutral collision frequency (Lathuillère et al., 1983; Johnson and Wickwar, 1987).

Because an excellent review paper has recently been published on energetics of the thermosphere (Killeen, 1987), we do not review the subject of Joule heating again in this paper. Instead, we concentrate on some specific aspects of each term in Equation [1]. We first consider the electric field, and show that seasonal change is significant in the electric field pattern and intensity observed from Sondrestrom (de la Beaujardière et al., 1988). We then consider the conductivities, and show that during solar maximum the solar-produced F region ionization can contribute more than 50% of the total height-integrated Pedersen conductivity. Finally, we make some remarks concerning the importance of the neutral wind contribution to Joule heating.

In this paper, data from the Sondrestrom and Chatanika incoherent scatter radars (Kelly, 1983, Leadabrand et al., 1972) are used. At 75° invariant latitude, Sondrestrom is usually in the polar cap during the night. It is in the cleft, cusp and auroral zone during the day. At 65° invariant latitude, Chatanika is usually in the auroral zone during the night, and equatorward of the auroral oval during the day.

SEASONAL DEPENDENCE OF HIGH-LATITUDE IONOSPHERIC CONVECTION

The dependence of high-latitude electric field on geomagnetic activity and IMF configuration has been studied for many years, using data from satellites and ground-based instruments (Heppner, 1977; Holt et al., 1987; Heppner and Maynard, 1987; Foster et al., 1971, 1986; Friis-Christensen et al., 1985; de la Beaujardière et al., 1985, 1986; de la Beaujardière and Wickwar, 1986; Holt et al., 1987). Little is known, however, about possible seasonal variations of electric fields. This is surprising, because it has been known for decades that the various indices of magnetic activity are seasonally dependent, with maxima in spring and fall (Cortie, 1912; Russell and McPherron, 1973, and references therein). Similarly, high-latitude ionospheric currents, and field aligned currents have maxima in summer (Matsushita and Xu, 1982; Campbell, 1982; Fujii et al., 1981). To our knowledge, a systematic analysis of the seasonal dependence of ionospheric electric fields has never been done before the work described here and in de la Beaujardière et al. (1988). Seasonal variations in plasma convection are important to assess in the context of Joule

heating calculations since the Joule heating rate is approximately proportional to the square of the ion velocity.

We have binned and averaged all the Sondrestrom data taken during experiments lasting more than 7 hours. The observations spanned five years, roughly centered around solar minimum, from March 1983 to July 1988. More than 130 days were averaged. The most salient points revealed by these studies and illustrated by Figures 1 to 3 can be summarized as follows:

- The equinox and summer convection velocities show a smooth two-cell pattern, whereas the winter convection velocity is comparatively disorganized.
- The winter East-West (E-W) component of the velocity is the largest in the dawn and noon sectors.
- The summer North-South (N-S) component is the smallest in the noon and dusk sectors.
- There is a phase difference in the daily variations of the E-W velocity component, the winter months leading equinoctial and summer months. Especially on the day side, this phase difference can be interpreted as a clockwise rotation of the convection pattern.
- In the noon portion of the afternoon cell, the latitude of the convection reversal from sunward to antisunward is highest during the summer months.
- In the dawn convection cell the latitude of the convection reversal from sunward to antisunward is highest during the winter months.

We now discuss some of these points in more details. Figures 1a through 1d show the average velocities. Thick and thin vectors are used to distinguish west and east velocities, respectively. The bin size is 1° by 1 hour, covering the invariant latitude interval from 67° to 82°. The number of points in each bin is typically 200 to 300. Comparing summer and winter data (Figures 1b and d), we see that the average convection is somewhat smoother and more regular in summer. This is not unexpected because, on individual winter days, and especially on the nightside, the convection has previously been reported to be highly irregular (Heppner, 1977). This is evidenced in the winter convection pattern shown, for example, by Heelis and Hanson (1980) and de la Beaujardière et al. (1985). However, the averaging of winter data presented here smoothes out much of the irregularity, and the winter drifts appear to maintain a somewhat erratic but fairly well organized two-cell convection pattern.

Figures 2a and 2b show the individual components of the plasma drift as a function of time for all seasons. (The data for this figure and the following one correspond to a 2° by 2 hour grid size.) The winter E-W component is largest between 05 and 15 LT, i.e., in the dawn and noon local time sectors. The summer N-S component is smallest between 09 and 17 LT, i.e., in the noon and most of the dusk local time sectors.

The latitude at which the convection reverses from sunward to antisunward is displayed in Figure 3. For this figure, the 2° × 2 hr averaged data were used. The latitude of this reversal has an opposite dependence on season in the dusk and dawn cells. In winter, the dusk cell has its convection reversal at, or equatorward of, the other seasons. In summer, the dawn cell has its convection reversal at, or equatorward of, the other seasons. In other words, the dusk convection reversal is at lowest latitudes during the winter, while the dawn convection reversal is at lowest latitudes during the summer. These latitudinal differences are most pronounced in the noon and midnight sectors.

Note that, for the summer curves, the afternoon reversal is beyond the field of view at noon when it is poleward of 81°. At midnight, the reversal is also beyond the field of view, but it is equatorward of 68°. The winter reversal is located equatorward of the summer reversal in the afternoon cell and poleward in the morning cell.

Because Joule heating is approximately proportional to the square of the electric field, or equivalently, to V^2, the individual drifts were also squared and averaged according to season. The

results of averaging all latitudes together are displayed in Figure 4 as a function of local time. The daily variations show three maxima which occur (1) one to two hours before local midnight; (2) at dawn; and (3) one to two hours after local noon. (At Sondrestrom, magnetic local time precedes local time by about one hour.) Except during summer, the largest values are those that occur before noon and before midnight. Part of these variations, however, are due to the offset between the geomagnetic and geographic poles. Over the course of one day, the Sondrestrom radar samples differing parts of the convection.

As stated by Foster et al. (1983), the seasonal differences in the square of the velocity are small. However, close examination of Figure 4 reveals that the small difference between seasons is probably significant. By averaging over all local times we find that V^2 is the smallest in summer ($V^2 = 1.6 \times 10^5$ m^2 s^{-2}) and largest in fall ($V^2 = 1.8 \times 10^5$ m^2 s^{-2}). Spring and winter are about equal. In fact, the same seasonal dependence is also apparent in Foster et al. (1983), who binned the square of the electric field measured from the Atmosphere Explorer C (AE-C) satellite during two time intervals close to the previous solar minimum. By inspecting their figure, reproduced here as Figure 5, it is clear that the squared electric field (E^2) is largest in fall and smallest in summer. Also, this difference is more pronounced during the quiet periods (K_p 0 to 3) than during the active periods (K_p 3 to 6). And indeed, these authors state that, overall, the E^2 is 20% lower in summer than in winter and equinox.

The differences in E^2 have repercussions in terms of Joule heating. Neglecting the neutral wind effects, Foster et al. (1983, Figure 7) find that during quiet times, the Joule heating rate integrated over all latitudes is maximum in fall. The higher conductivities resulting from the larger solar illumination during summer are not sufficient to offset the fact that E^2 is smaller in summer than in the fall.

CONDUCTIVITIES FROM SOLAR-PRODUCED IONIZATION

The Hall and Pedersen conductivities are given by:

$$\sigma_P = \frac{N_e e}{B}\left[\frac{\nu_{en}\Omega_e}{\nu_{en}^2+\Omega_e^2} + \frac{\nu_O\Omega_O}{\nu_O^2+\Omega_O^2}p_O + \frac{\nu_{NO}\Omega_{NO}}{\nu_{NO}^2+\Omega_{NO}^2}p_{N_2} + \frac{\nu_{O_2}\Omega_{O_2}}{\nu_{O_2}^2+\Omega_{O_2}^2}p_{O_2}\right] \quad (2)$$

$$\sigma_H = \frac{N_e e}{B}\left[\frac{\Omega_e^2}{\nu_{en}^2+\Omega_e^2} - \frac{\Omega_O^2}{\nu_O^2+\Omega_O^2}p_O - \frac{\Omega_{NO}^2}{\nu_{NO}^2+\Omega_{NO}^2}p_{N_2} - \frac{\Omega_{O_2}^2}{\nu_{O_2}^2+\Omega_{O_2}^2}p_{O_2}\right] \quad (3)$$

where:

N_e is the electron density

e is the charge of electron

ν_{en} is the electron-neutral collision frequency

$\nu_O, \nu_{O_2}, \nu_{NO}$ are the ion-neutral collision frequencies

Ω_e is the electron gyrofrequency

$\Omega_O, \Omega_{O_2}, \Omega_{NO}$ are the ion gyrofrequencies

p_O, p_{O_2}, p_{N_2} are the relative ion concentrations

Recently, Brekke and Hall (1988) reviewed conductivity measurements and empirical models. Listing the various terms in Equations [2] and [3], they described the simplifying assumptions that are often made in calculating the Hall and Pedersen conductivities. In particular, these

authors stressed that the collision-frequency models adopted are of great importance when deriving the conductivity.

Brekke and Hall (1988) also helped clarify the dependence of conductivities on the solar zenith angle (χ). While several authors have stated that the Pedersen and Hall conductivities (Σ_p and Σ_H) are proportional to $\cos\chi$, others have argued that conductivities are proportional to $(\cos\chi)^{0.5}$, or, more generally, to $(\cos\chi)^n$. Brekke and Hall (1988) showed that the conductivities are better described using an expression where the two terms in $\cos\chi$ are added. They obtained for the Pedersen and Hall conductivities an expression of the form: $\Sigma = a\cos\chi + b(\cos\chi)^{0.5}$. Adding these two terms is justified by the fact that, in the lower E region, the ionization recombination process is dominated by dissociative recombination, so the electron density is proportional to $\cos\chi$; whereas in the upper E region and in the F region, charge exchange processes dominate and the electron density is proportional to $(\cos\chi)^{0.5}$.

In another recent article, Rasmussen et al. (1988) studied, among other things, the height-dependent Pedersen conductivities. They calculated how much of the height-integrated Pedersen conductivity originates from F region altitudes (above ~170 km) and how much originates from the E region. These authors showed that, during solar maximum conditions, the F region can contribute more than previously assumed. They derived the values of the ionospheric densities and conductivities from the combination of a photochemical equilibrium model at E-region altitudes, and the full F-region model including transport and diffusion at higher altitudes. Under solar maximum conditions, they concluded, the contribution to Σ_p from the ionosphere above 170 km can reach 40% during day-time and 80% at dusk. Comparison of their ionospheric density model with incoherent scatter data shows that in the altitude range 110 to 200 km, the predicted values are underestimated by 40 to 50%. It is therefore important to assess, using actual data, the F region contribution to height integrated conductivities.

We have examined Chatanika and Sondrestrom ionospheric density measurements and calculated the conductivities (Equations [2] and [3]) without making the approximations that have often been made in the past. The procedure was the same as used for the Chatanika data in Rasmussen et al. (1988), and we looked at all the days that were analyzed by these authors. All the collision terms between electrons, NO^+, O_2^+, O^+ and N_2, O_2, O were included, using the collision frequencies in Schunk and Nagy (1980). The neutral atmosphere was obtained from the MSIS-83 model (Hedin et al., 1983). The results are shown in Figures 6a through 6c where the solid and dashed lines represent Pedersen conductivity integrated up to 500 and 180 km altitudes, respectively. Figure 6a is for solar cycle minimum ($S_{10.7}$= 69); Figures 6b and 6c are for solar cycle maximum ($S_{10.7}$ = 197 and 180, respectively).

Qualitatively, these calculations agree with Rasmussen et al. (1988). During solar cycle minimum the difference between the two curves is very small, indicating that the F-region contribution to Σ_p is small, less than ~10%. During solar cycle maximum, the difference can be larger. Figure 6b shows a large F-region contribution, reaching 60%, during the daytime hours. Although it is daytime, the sun has a razing incidence and the solar zenith angle always exceeds 80° with the result that the rate of EUV photoionization is small in the E region and large in the F region. This corresponds to the dusk conditions described by Rasmussen et al. (1988) when the F-region contribution is largest. However, this contribution is smaller than that obtained from the model calculation, which was 80%. Figure 6c shows a much smaller F-region contribution than Figure 6b, about 20%. In this case the solar zenith angle is smaller, giving rise to a larger E-region contribution to the Pedersen conductivity. This is again in qualitative agreement with Rasmussen et al. (1988), but as in Figure 6b, the F-region contribution is smaller than that obtained from the model calculation.

In order to asses the relative importance of each element in the conductivity calculation (Equations [2] and [3]), we show in Figures 7a, 7b, and 8 the height profiles of the Hall and Pedersen conductivities and of the electron density. The time is local noon, and the day selected is February 4, 1981, the day illustrated in Figure 6b for which the F region contribution to the

Pedersen conductivity was large. Figure 7a shows that the contribution to the Pedersen conductivity from the electrons (the first term in Equation [2]) is negligible at all altitudes above 90 km. The contribution from the molecular ions (last two terms in Equation [2]) dominates up to about 190 km. The contribution from atomic oxygen ions (second term in Equation [2]) dominates above 190 km. This is because the electron density was extremely large in the F region (1.8×10^6 el/cm^3), whereas it was very small in the E region (5.3×10^4 el/cm^3).

The components of the Hall conductivity are displayed in Figure 7b. The Hall conductivity is the difference between the contribution from the electrons (first term in Equation [3]) and from the ions (three other terms in Equation [3]). The conductivity peaks at 112 km, slightly below the E-region peak at 120 km. Below the peak, σ_H depends mostly on the electron term; above the peak, molecular ions determine the shape of the curve. The contribution from atomic oxygen is negligible at all heights.

NEUTRAL WIND

The final parameter we would like to comment on is the neutral wind, **U**. Equation 1 shows that the Joule heating of the neutral atmosphere is proportional to the square of the vector difference between the ion drift and the neutral wind. Because few techniques can provide the **V** and **U** vectors simultaneously, and because **U** is generally smaller than the **E** × **B** drift, the neutral wind is often ignored. However, its contribution can be quite important. In the F region, ion drag tends to diminish the size of **V**- **U**; and in the E region, the wind can be very large during geomagnetically active conditions (Brekke and Rino, 1978; Johnson and Wickwar, 1987; Baron and Wand, 1983). Depending on the magnitudes of the ion and the neutral velocities, as well as the time history of a particular event, the Joule heating rate can be either reduced or enhanced relative to the **U** = 0 value.

The incoherent scatter technique provides the electric field at all heights. This technique also allows both components of **U** to be determined in the E region, and the meridional component of **U** to be determined in the F region (Johnson, 1988). Joule heating rates derived from Chatanika radar measurements using Equation [1] are displayed in Figure 9. These observations show an example of the magnitude of the neutral wind effect on a highly disturbed day characterized by large electric fields and intense particle precipitation. The two curves on this figure show the local Joule heating rates at 115 km altitude. The solid line is derived from Equation 1, and the dashed line computed by setting the neutral wind equal to zero. The observations correspond to the period illustrated in Figure 6c (June 10-11, 1980). As this particular example shows, the Joule heating rate that includes the neutral wind effect is generally 2 to 4 times less than the rate derived by assuming **U** = 0. The decrease is highly variable, however, and at times approaches or exceeds a factor of 10. After 20 UT (10 LT) the Joule heating rate derived by assuming **U** = 0 is actually exceeded by that obtained by including the neutral wind. This follows a rapid change in the direction and magnitude of ion convection, which is not immediately reflected in the neutral flow because the neutral atmosphere responds slowly to changes in the ion flow.

This result shows that the effect of neutral winds on the local Joule heating rate is nonnegligible and can at times dominate. During most of the time illustrated, the calculated Joule heating, on the average, is 2 to 4 times smaller when the neutral wind is included than when it is set to zero.

The neutral winds have seasonal variations (Roble 1983; Wickwar et al., 1986) that have not been considered in this study. These variations must also be reflected in the seasonal variation of Joule heating.

SUMMARY OF OBSERVATIONS

In this paper we have focused on the three physical parameters – the electric field, the Pedersen conductivity, and the neutral wind – that determine the Joule heating rate. Summarized below are some significant findings.

- The data presented here and in de la Beaujardière et al. (1988) indicate that the intensity of the ionospheric electric field, as well as the average convection pattern, are different for each season. The magnitude of the plasma convection is smallest in summer and largest in fall.
- During quiet geomagnetic conditions, the Joule heating rate is maximum in the fall.
- The F-region contributes little to nighttime integrated Pedersen conductivities. During the daytime, under solar maximum conditions, the F-region conductivity can be larger than the E-region conductivity.
- The often-neglected neutral wind can be important. In our example, the Joule heating, calculated by incorporating the actual neutral wind values, was generally 2 to 4 times smaller than that calculated by assuming $\mathbf{U} = 0$. The reverse can also be true, as was illustrated during a period when the wind was larger than the $\mathbf{E} \times \mathbf{B}$ drift.

DISCUSSION

An inherent limitation in averaging all data by season as we have done here is that we smooth out all levels of magnetic activity and of IMF B_z and B_y, all of which profoundly affect ionospheric plasma convection. However, the present study gave enough points in each bin so that the results are statistically significant. With time we will accumulate enough measurements to calculate separate empirical models as a function of season, magnetic activity and IMF.

As shown by Equation [2] and Figure 7b, the F region Pedersen conductivity depends on the collision frequency between neutrals and O^+ ions. However, it is becoming increasingly clear that the values of O^+/O collisional cross section that are generally adopted may have to be altered. As is pointed out by Burnside et al. (1987) the value commonly adopted may have to be multiplied by as much as 1.7. If this were the case, the F-region Pedersen conductivity would also have to be increased, since O^+ ions dominate at this altitude (see Figure 7a). This will increase even more the relative contribution from the F region to the integrated Pedersen conductivity.

The large F region conductivity has important consequences in terms of high latitude electrodynamics: (1) Over a significant fraction of the F layer, the ions do not move in the $\mathbf{E} \times \mathbf{B}$ direction, but rather, collisions have the effect of deflecting them in the direction of $\mathbf{E}$. (2) The ionospheric current vector, $\mathbf{J}_\perp$, rotates by 90° between the E and F layers. $\mathbf{J}_\perp$ is perpendicular to the electric field in the E region, and parallel in the F region. (3) A large fraction of the field-aligned current closure by Pedersen current occurs in the F region.

Our last point concerns the role of the neutral wind in Joule dissipation. The energy dissipated to the neutrals is governed by Equation [1], and, as we have shown, the neutral wind term should not be neglected in the calculation. When dealing with the magnetosphere, however, the actual energy dissipated by Joule heating is evaluated by considering only the electric field and by not including the neutral wind term (Sugiura, 1984; Vasyliunas, 1970).

ACKNOWLEDGMENTS

This work was supported by NSF Cooperative Agreement ATM-8516436, AFGL Contract F19628-87-K006, and AFOSR contract F49620-87-K-0007.

REFERENCES

Baron, M. J., and R. H. Wand, F-region ion temperature enhancements resulting from Joule heating, *J. Geophys. Res.*, *88*, 4114-4118, 1983.

Baumjohann, W., and Y. Kamide, Hemispherical Joule heating and the AE indices, *J. Geophys. Res.*, *89*, 383, 1984.

Brekke, A., and C. L. Rino, High-resolution altitude profiles of the auroral zone energy dissipation due to ionospheric currents, *J. Geophys. Res.*, *83*, No. A6, 2517-2524, 1978.

Brekke, A., and C. Hall, Auroral ionospheric quiet summer time conductances, *Ann. Geophys.*, *6*, 361-376, 1988.

Burnside, R. G., C. A. Tepley, and V. B Wickwar, The O^+-O collision cross section: can it be inferred from aeronomical measurements?, *Ann. Geophys.*, 5A, 342-350, 1987.

Campbell, W. H., Annual and semiannual changes of the quiet daily variations (Sq) in the geomagnetic field at North American locations, *J. Geophys. Res.*, *87*, No. A2, pp. 785-796, 1982

Cortie, A. L., Sunspots and terrestrial magnetic phenomena, 1898-1911, *Mon. Notic. Roy. Astron. Soc.*, *73*, 52-60, 1912.

de la Beaujardière, O., V. B. Wickwar, J. D. Kelly, and J. H. King, IMF-B_y effects on the high-latitude nightside convection, *Geophys. Res. Lett.*, *12*, 461-464, 1985.

de la Beaujardière, O., and V. B. Wickwar, IMF control of plasma drift, ion temperature and neutral wind, *Proceedings of the U.S.-Finland Auroral Workshop*, 1986.

de la Beaujardière, O., V. B. Wickwar, and J. H. King, Sondrestrom radar observations of the effect of the IMF B_y component on polar cap convection, in *Solar Wind-Magnetosphere Coupling*, edited by Kamide and Slavin, eds., 495-505, Terra/Reidel Publishing Company, Tokyo, 1986.

de la Beaujardière, O., et al., Seasonal dependence of high-latitude ion convection, to be submitted to *J. Geophys. Res.*, 1988.

Evans, D. S., N. C. Maynard, J. Troim, T. Jacobsen, and A. Egeland, Auroral vector electric field and particle comparison. 2. Electrodynamics of an arc, *J. Geophys. Res.*, *82*, 2235, 1977.

Foster, J. C., D. H. Fairfield, K. W. Ogilvie, and T. J. Rosenberg, Relationship of interplanetary parameters and occurrence of magnetospheric substorms, *J. Geophys. Res.*, *76*(28), 6971-6975, 1971.

Foster, J. C., J.-P. St.-Maurice, and V. J. Abreu, Joule heating at high latitudes, *J. Geophys. Res.*, *88*, 4885-4896, 1983.

Foster, J. C., J. M. Holt, R. G. Musgrove, and D. S. Evans, Ionospheric convection associated with discrete levels of particle precipitation, *Geophys. Res. Lett.*, *13*, 656-659, 1986.

Friis-Christensen, E., Y. Kamide, A. D. Richmond, and S. Matsushita, interplanetary magnetic field control of high-latitude electric fields and currents determined from Greenland magnetometer data, *J. Geophys. Res.*, *90*, 1325, 1985.

Fujii, R., T. Iijima, T. A. Potemra, and M. Sugiura, Seasonal dependence of large-scale Birkeland currents, *Geophys. Res. Lett.*, *8*, 1103-1106, 1981.

Hedin, A. E., A revised thermospheric model based on mass spectrometer and incoherent scatter data: MSIS-83, *J. Geophys. Res.*, *88*, 10170-10188, 1983.

Heelis, R. A., and W. B. Hanson, High-latitude ion convection in the nighttime F region, *J. Geophys. Res.*, *85*, 1995, 1980.

Heppner, J. P., Empirical models of high-latitude electric fields, *J. Geophys. Res.*, *82*, 1115, 1977.

Heppner, J. P., and N. C. Maynard, Empirical high-latitude electric field models, *J. Geophys. Res.*, *92*, 4467-4489, 1987.

Holt, J. M., R. H. Wand, J. V. Evans, and W. L. Oliver, Empirical models for the plasma convection at high latitudes from Millstone Hill observations, *J. Geophys. Res.*, *92*, No. A1, 203-212, 1987.

Johnson, R. M., and V. B. Wickwar, Incoherent scatter measurements of high-latitude lower-thermospheric density and dynamics. In press, *Proceedings of the Atmospheric Density and Aerodynamic Drag Workshop*, AFGL, October 10, 1987.

Johnson, R. M., Lower-thermospheric neutral winds at high-latitude determined from incoherent scatter measurements: A review of techniques and observations, in press, *Advances in Space Research*, 1988.

Kelly, J. D., Sondrestrom radar-initial results, *Geophys. Res. Letts.*, *10*, 1112-1115, 1983.

Killeen, T. L., Energetics and dynamics of the earth's thermosphere, *Rev. Geophys.*, *25*, No. 3, 433-454, 1987.

Lathuillère, C., V. B. Wickwar, and W. Kofman, Incoherent scatter measurements of ion-neutral collision frequencies and temperatures in the lower thermosphere of the auroral region, *J. Geophys. Res.*, *88*, No. A12, 10137-10144, 1983,

Leadabrand, R. L., M. J. Baron, J. Petriceks, and H. F. Bates, Chatanika, Alaska, auroral-zone incoherent-scatter facility, *Radio Sci.*, *7*, No. 7, 747-756, 1972.

Matsushita, S., and W.-Y. Xu, Equivalent ionospheric current systems representing IMF sector effects on the polar geomagnetic field, *Planet. Space Sci.*, *30*, No. 7, pp. 641-656, 1982.

Prolss, G. W., Magnetic storm associated perturbations of the upper atmosphere: Recent results obtained by satellite-borne gas analyzers, *Rev. Geophys. Space Phys.*, *18*, 183, 1980.

Rasmussen, C. E., R. W. Schunk, and V. B. Wickwar, A photochemical equilibrium model for ionospheric conductivity, *J. Geophys. Res.*, *93*, 9831, 1988.

Roble, R. G., R. E. Dickinson, and E. C. Ridley, Seasonal and solar cycle variations of the zonal mean circulation in the thermosphere, *J. Geophys. Res.*, *82*, 5493, 1977.

Roble, R. G., Dynamics of the earth's thermosphere, *Rev. Geophys. Space Phys.*, *21*, 217-233, 1983.

Russell, C. T., and R. L. McPherron, Semiannual variation of geomagnetic activity, *J. Geophys. Res.*, *78*, No. 1, 92-108, 1973.

Schunk, R. W., and A. F. Nagy, Ionospheres of the terrestrial planets, *Rev. Geophys.*, *18*, 813-852, 1980.

Sugiura, M., A fundamental magnetosphere-ionosphere coupling model involving field-aligned currents as deduced from DE-2 observations, *Geophys. Res. Lett.*, *11*, 877, 1984.

Vasyliunas, V. M., Mathematical models of magnetospheric convection and its coupling to the ionosphere, in *Particles and Fields in the Magnetosphere*, ed. by B. M. McCormac, *60*, Reidel, Hingham, Massachusetts, 1970.

Vickrey, J. F. R. R. Vondrak, and S. J. Matthews, Energy deposition by precipitating particles and Joule dissipation in the auroral ionosphere, *J. Geophys. Res.*, *87*, 5184, 1982.

Wickwar, V. B., O. de la Beaujardière, and C. A. Leger, The analysis phase of MITHRAS, Final Report, Air Force Office of Scientific Research Contract F49620-83-K-0005, SRI Project 4995, SRI International, Menlo Park, California, June 1986.

Fig. 1. Average ion convection velocities for (a) spring; (b) summer; (c) fall; (d) winter. The Sondrestrom data from March 1983 to July 1988 were averaged into 1° by 1hr bins. Local time is indicated on the outside and UT on the inside of the clock dial circle.

Fig. 2. Components of the average ion velocities at 75° invariant latitude with (a) eastward and (b) northward velocities. Note that the velocity scale for (a) is half that for (b). The error bar indicates the mean standard deviation. Fall and equinox have been averaged together.

Fig. 3. Latitude of the ion convection reversal for three seasons. This reversal is that of the 2°×2hr averaged data. Reversals in the morning and afternoon convection cell are indicated by separate curves, and the discontinuities in the noon and midnight local times show where the transition takes place. Arrows indicate where the convection reversal is located beyond the radar field of view.

Fig. 4. Average of squared ion velocity vectors as a function of local time for (a) fall and summer (solid and dotted lines, respectively); and (b) winter and spring (thick and thin lines, respectively).

Fig. 5. Average patterns of the squared electric field magnitude measured by binning AE-C data (from Foster et al., 1983).

Fig. 6. Pedersen height-integrated conductivity versus time measured during (a) solar minimum at Sondrestrom and (b) and (c) solar maximum at Chatanika. The solid curve shows the Pedersen conductivity integrated up to a 500-km altitude, and the dashed curve is for a 180-km altitude limit. The solar zenith angle is indicated at the top of the plots.

Fig. 7. Height profiles of the four components of (a) Hall conductivity and (b) Pedersen conductivity (see Equations [2] and [3].) The data correspond to 14 LT (00 UT) on February 4, 1981, illustrated in Figure 6b.

Fig. 8. Electron density profile corresponding to the Figure 7 conductivities.

Fig. 9. Joule heating rates at a 115-km altitude calculated neglecting (solid curve) and including (dashed curve) the effect of the neutral wind. The data correspond to June 11, 1980, illustrated in Figure 6c.

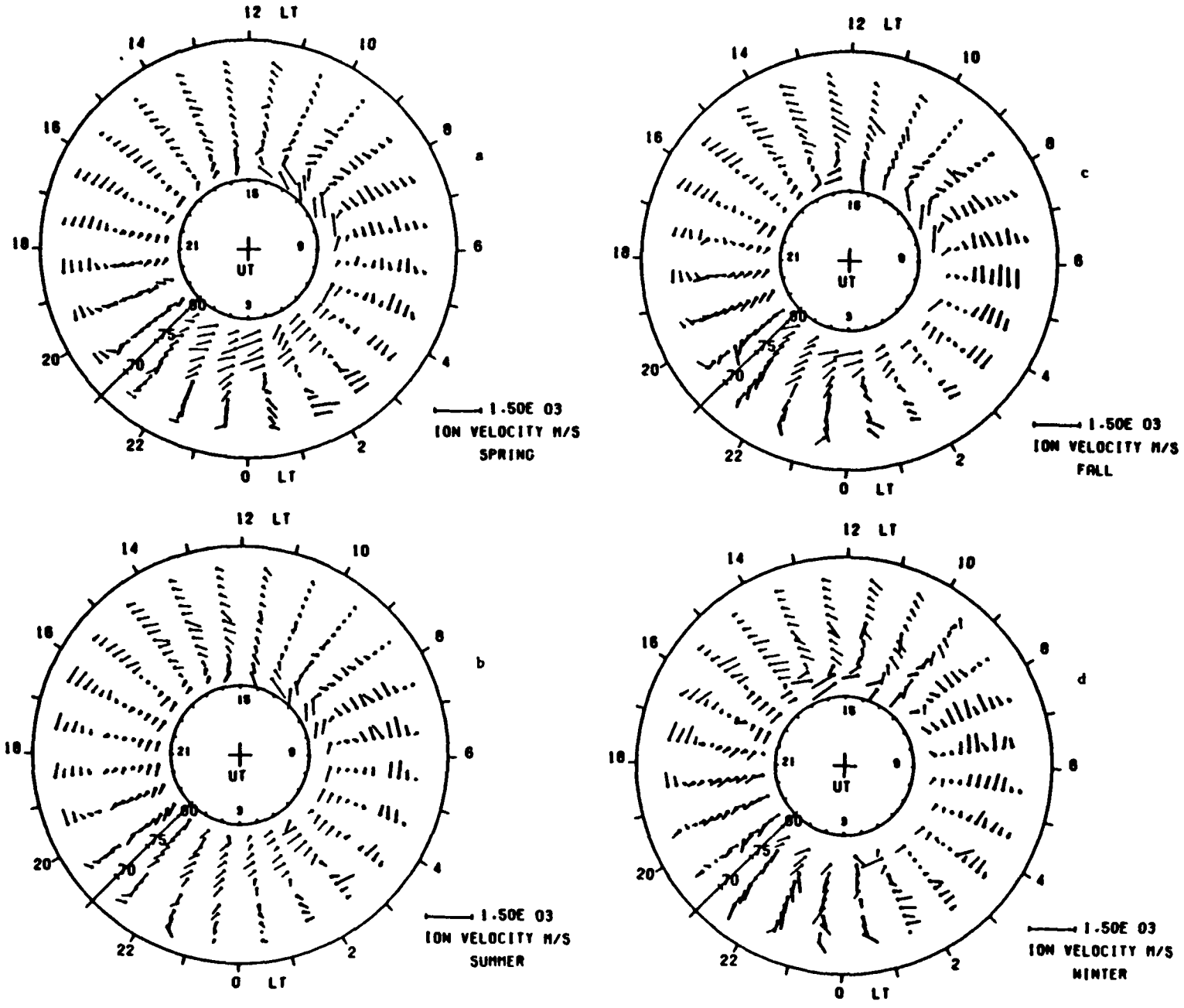
12 LT
14
10
16
8
18
6
20
4
22
2
0 LT
UT
60
75
70
a
1.50E 03
ION VELOCITY M/S
SPRING
c
FALL
b
SUMMER
d
WINTER

Fig. 1

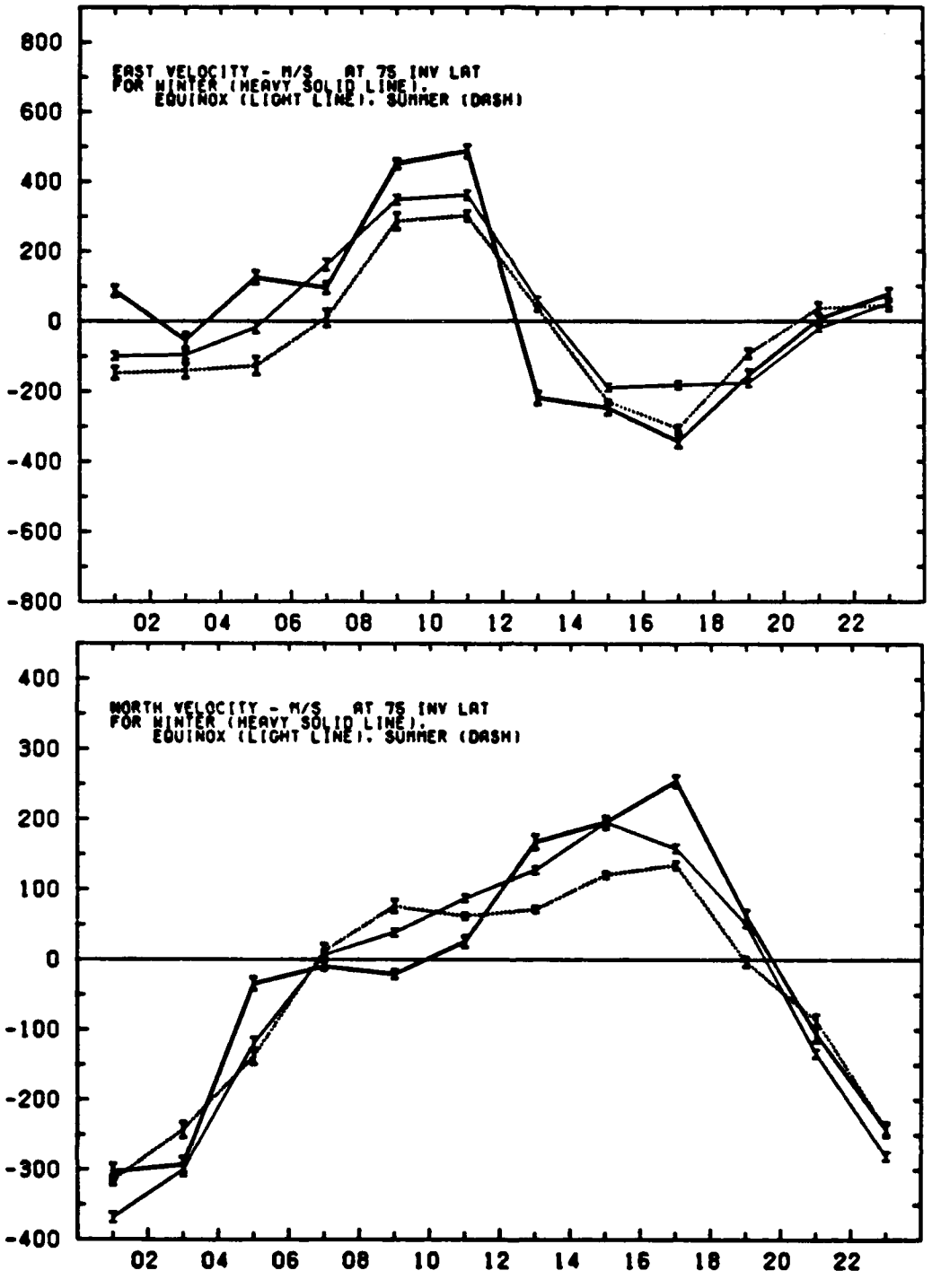
EAST VELOCITY - M/S AT 75 INV LAT
FOR WINTER (HEAVY SOLID LINE),
EQUINOX (LIGHT LINE), SUMMER (DASH)
800
600
400
200
0
-200
-400
-600
-800
02
04
06
08
10
12
14
16
18
20
22
NORTH VELOCITY - M/S AT 75 INV LAT
FOR WINTER (HEAVY SOLID LINE),
EQUINOX (LIGHT LINE), SUMMER (DASH)
400
300
200
100
0
-100
-200
-300
-400
02
04
06
08
10
12
14
16
18
20
22

Fig. 2

Seasonal Variations of Convection Reversal

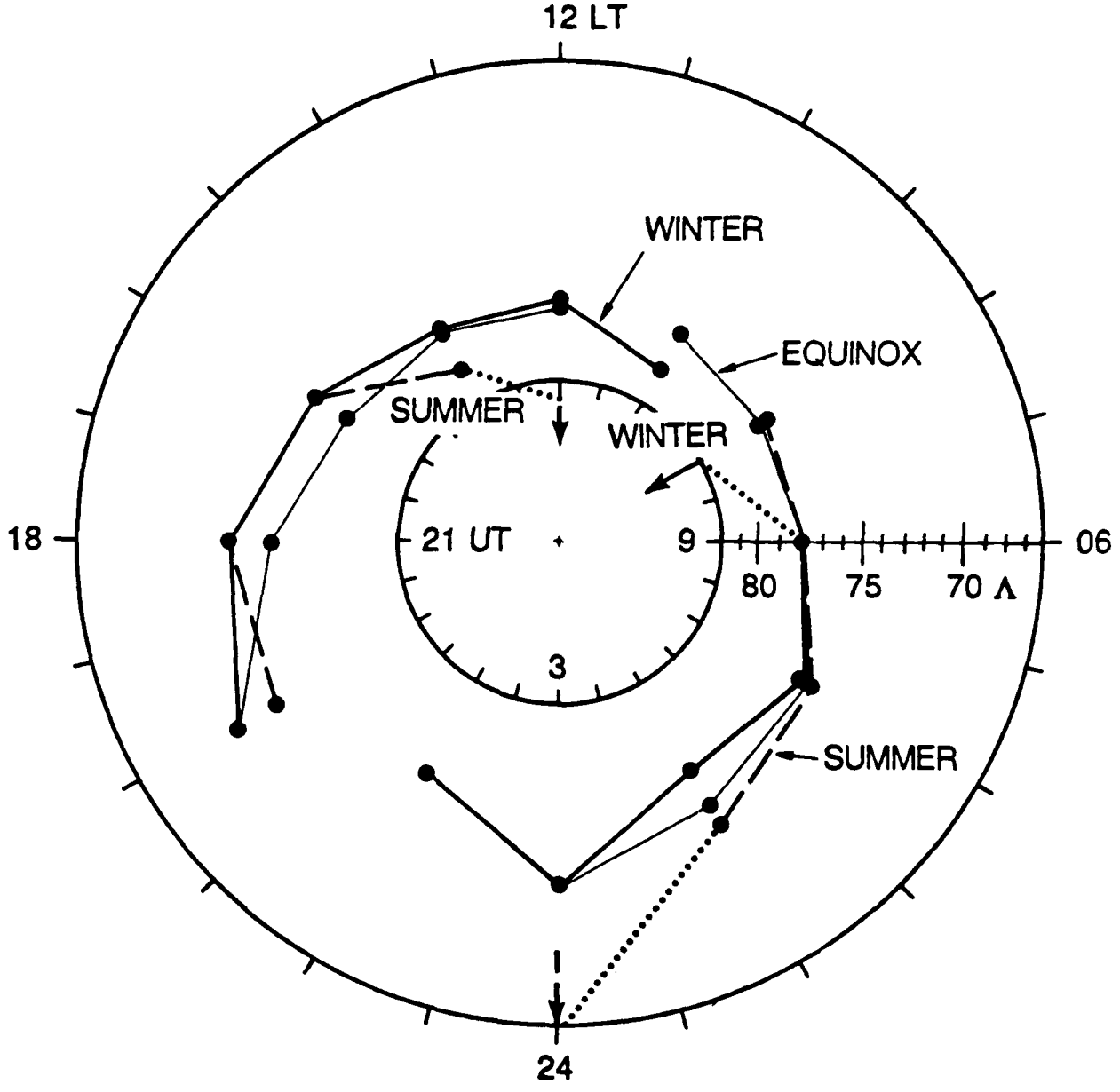

Fig. 3

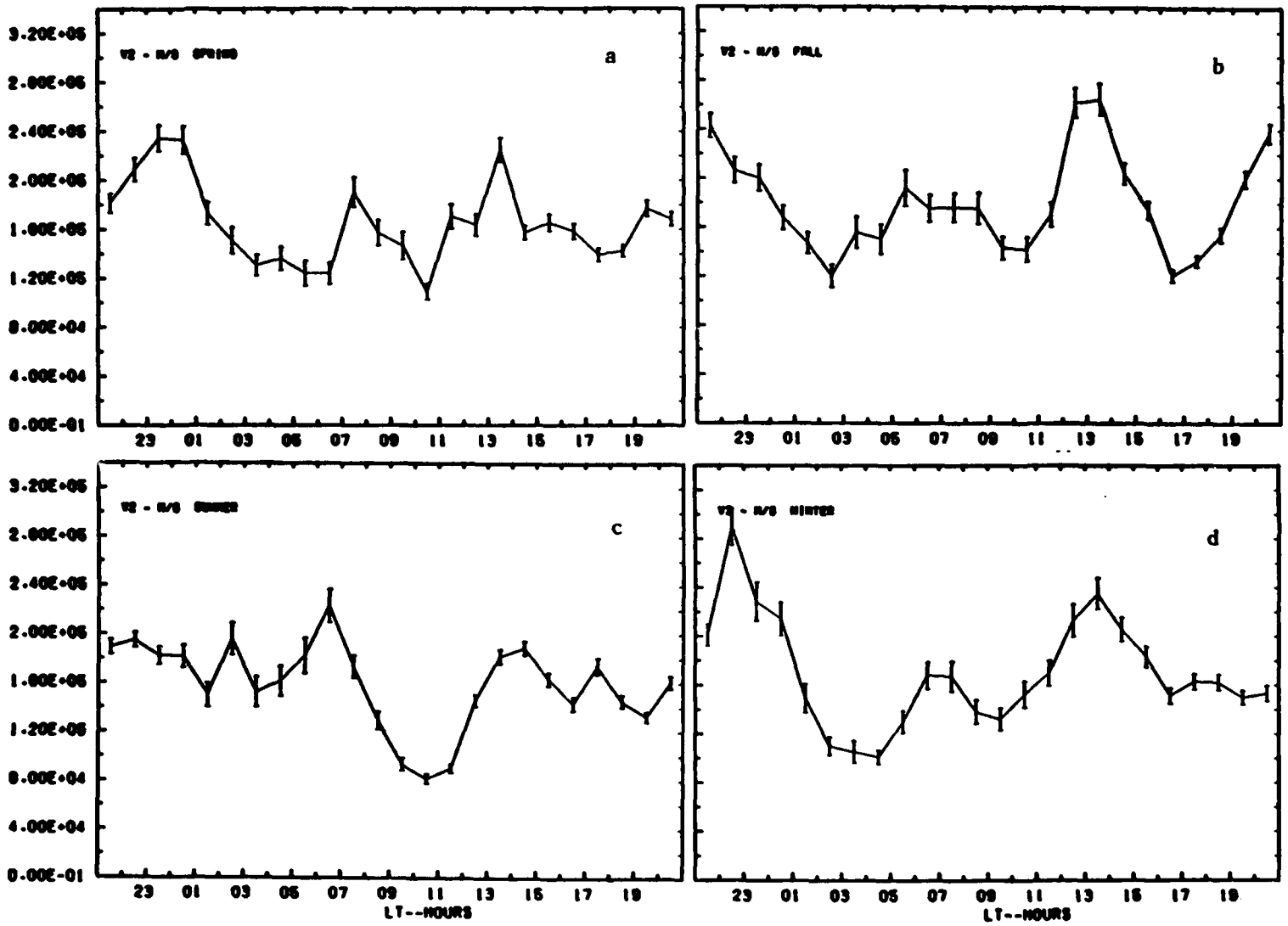

Fig. 4

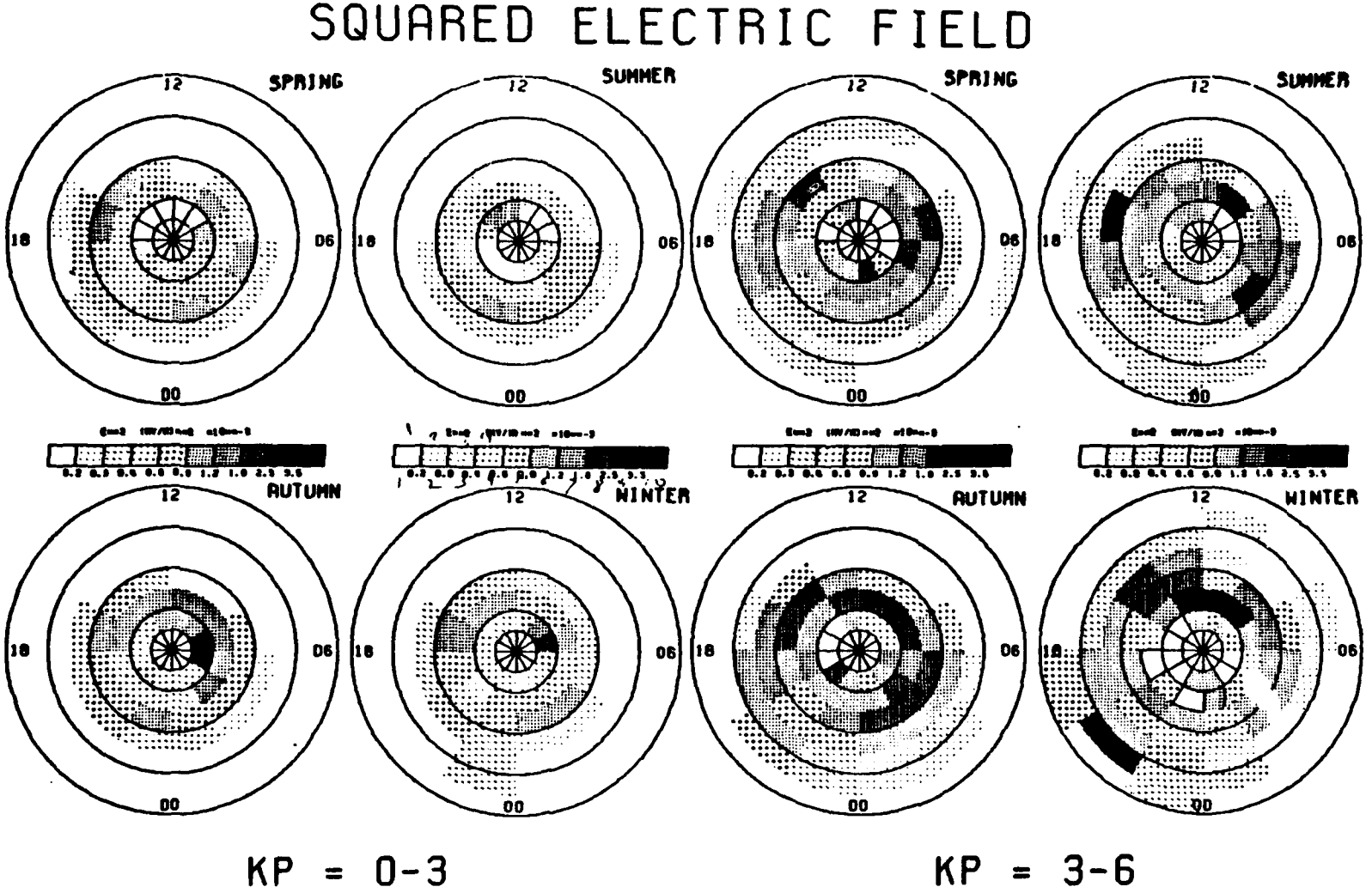
SQUARED ELECTRIC FIELD
SPRING
SUMMER
SPRING
SUMMER
AUTUMN
WINTER
AUTUMN
WINTER
12
18
06
00
KP = 0-3
KP = 3-6

Fig. 5

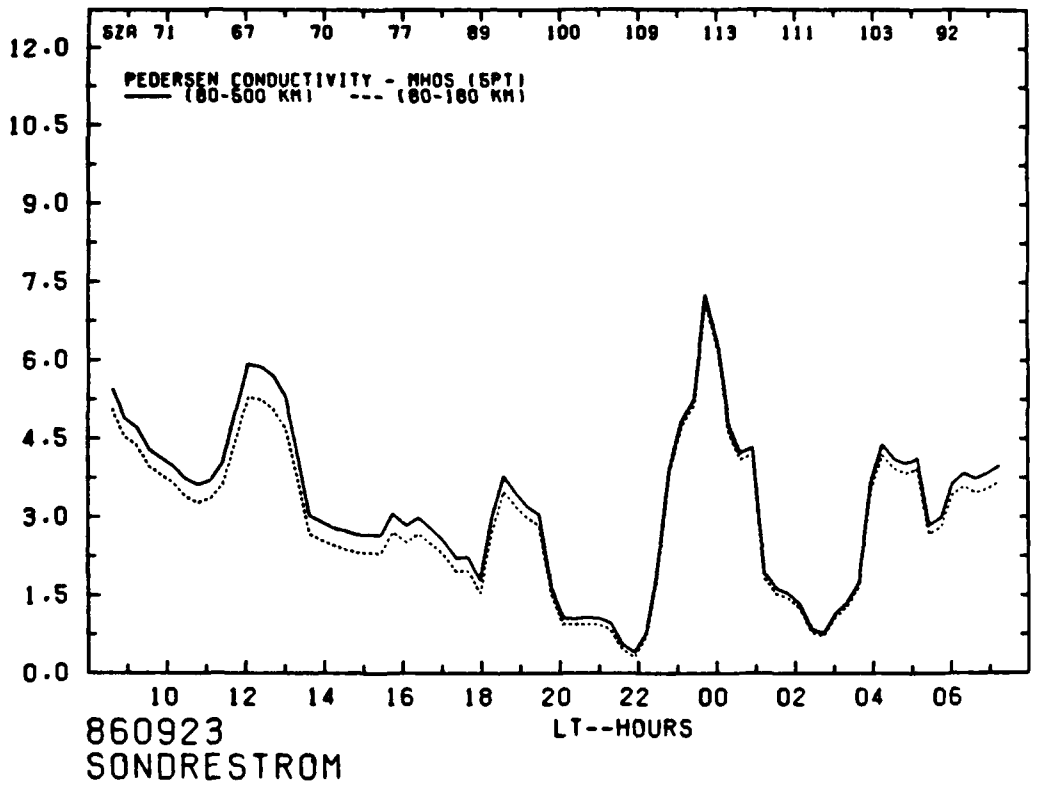
SZA 71 67 70 77 89 100 109 113 111 103 92
PEDERSEN CONDUCTIVITY - MHOS (SPT)
(80-500 KM) --- (80-180 KM)
12.0
10.5
9.0
7.5
6.0
4.5
3.0
1.5
0.0
10 12 14 16 18 20 22 00 02 04 06
LT--HOURS
860923
SONDRESTROM

Fig. 6 a

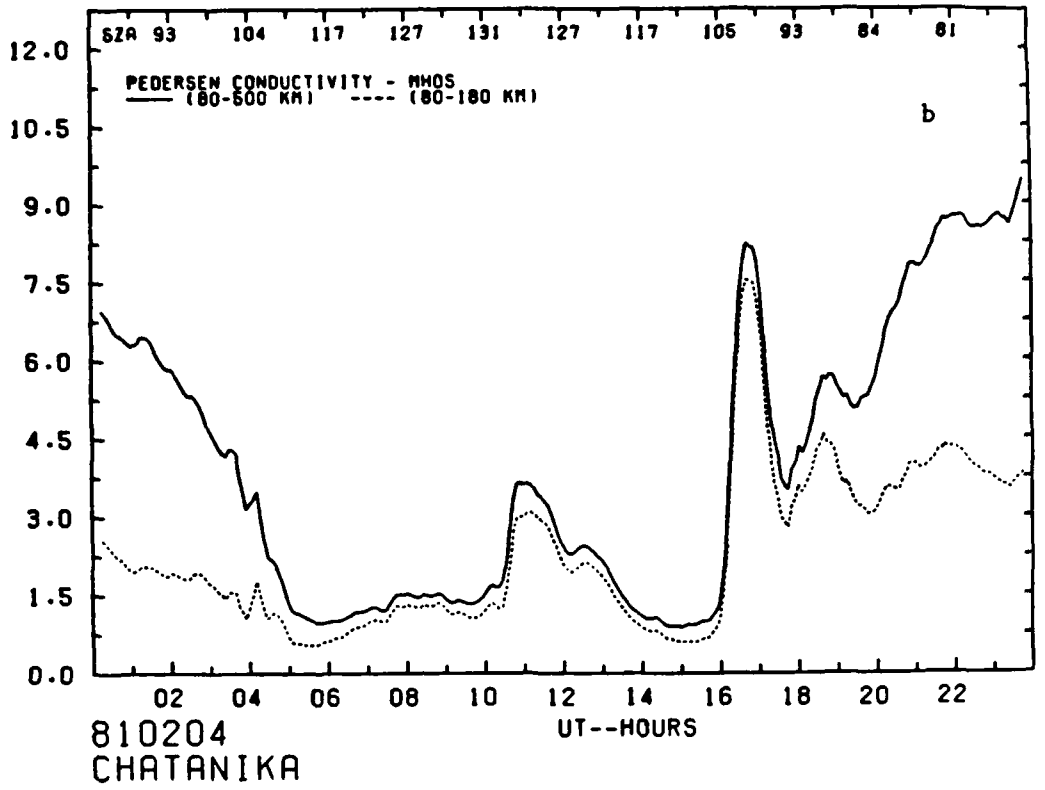
SZA 93 104 117 127 131 127 117 105 93 84 81
PEDERSEN CONDUCTIVITY - MHOS
(80-500 KM) (80-180 KM)
b
12.0
10.5
9.0
7.5
6.0
4.5
3.0
1.5
0.0
02 04 06 08 10 12 14 16 18 20 22
UT--HOURS
810204
CHATANIKA

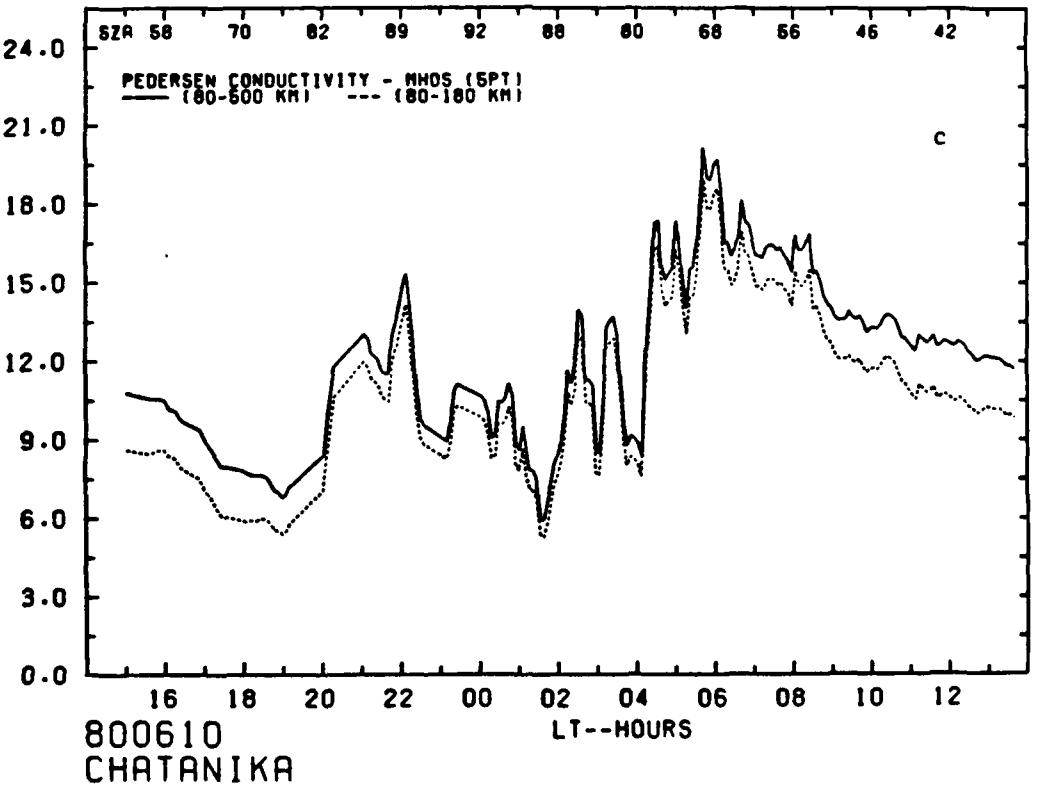
SZA 58 70 82 89 92 88 80 68 56 46 42
PEDERSEN CONDUCTIVITY - MHOS (5PT)
(80-500 KM) (80-180 KM)
c
24.0
21.0
18.0
15.0
12.0
9.0
6.0
3.0
0.0
16 18 20 22 00 02 04 06 08 10 12
LT--HOURS
800610
CHATANIKA

Fig. 6 b, c

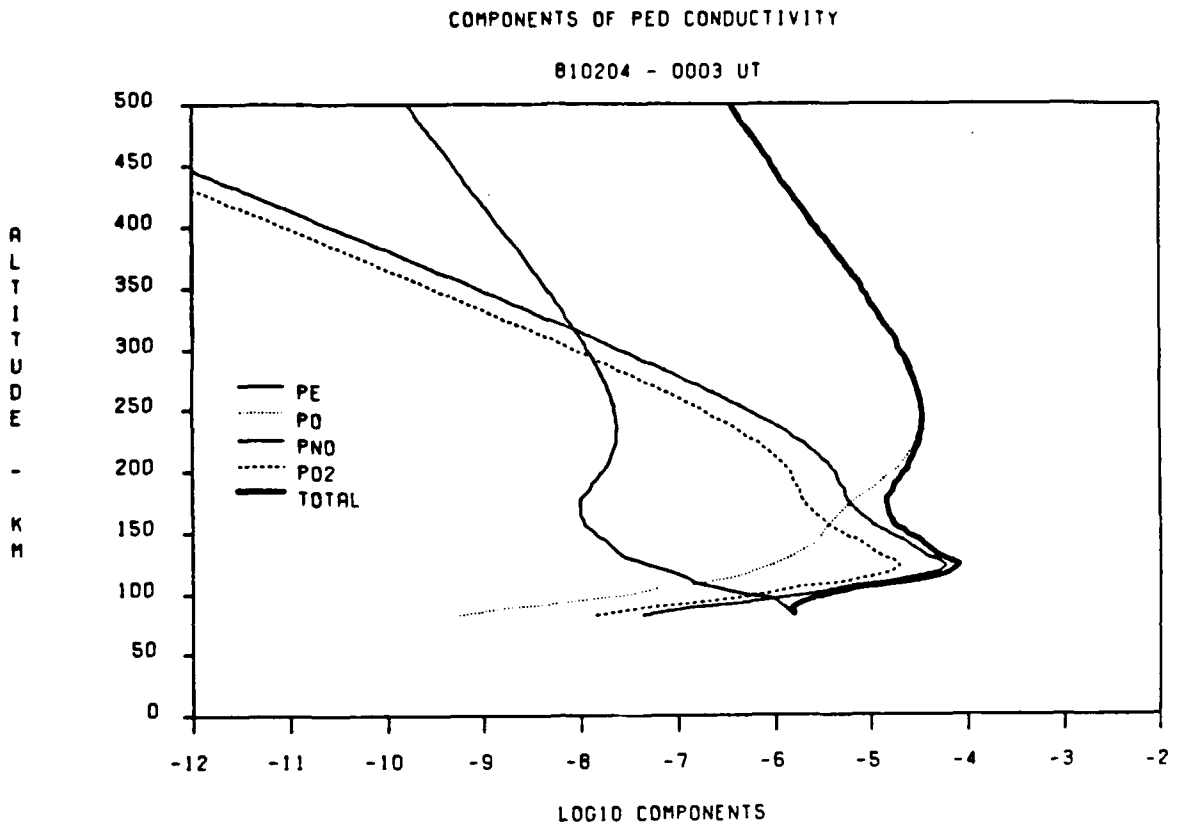
COMPONENTS OF PED CONDUCTIVITY
810204 - 0003 UT
ALTITUDE - KM
500
450
400
350
300
250
200
150
100
50
0
PE
PO
PNO
PO2
TOTAL
-12
-11
-10
-9
-8
-7
-6
-5
-4
-3
-2
LOG10 COMPONENTS

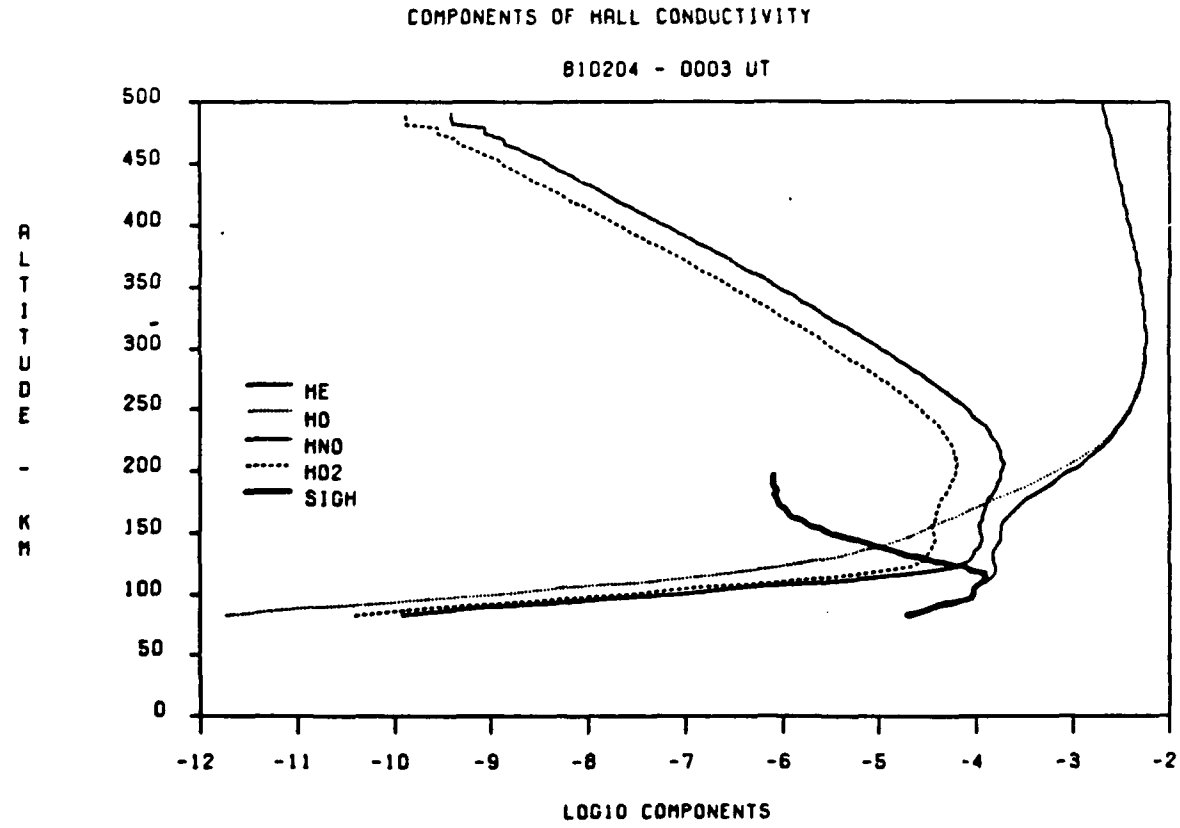
COMPONENTS OF HALL CONDUCTIVITY
810204 - 0003 UT
ALTITUDE - KM
500
450
400
350
300
250
200
150
100
50
0
HE
HO
HNO
HO2
SIGH
-12
-11
-10
-9
-8
-7
-6
-5
-4
-3
-2
LOG10 COMPONENTS

Fig. 7

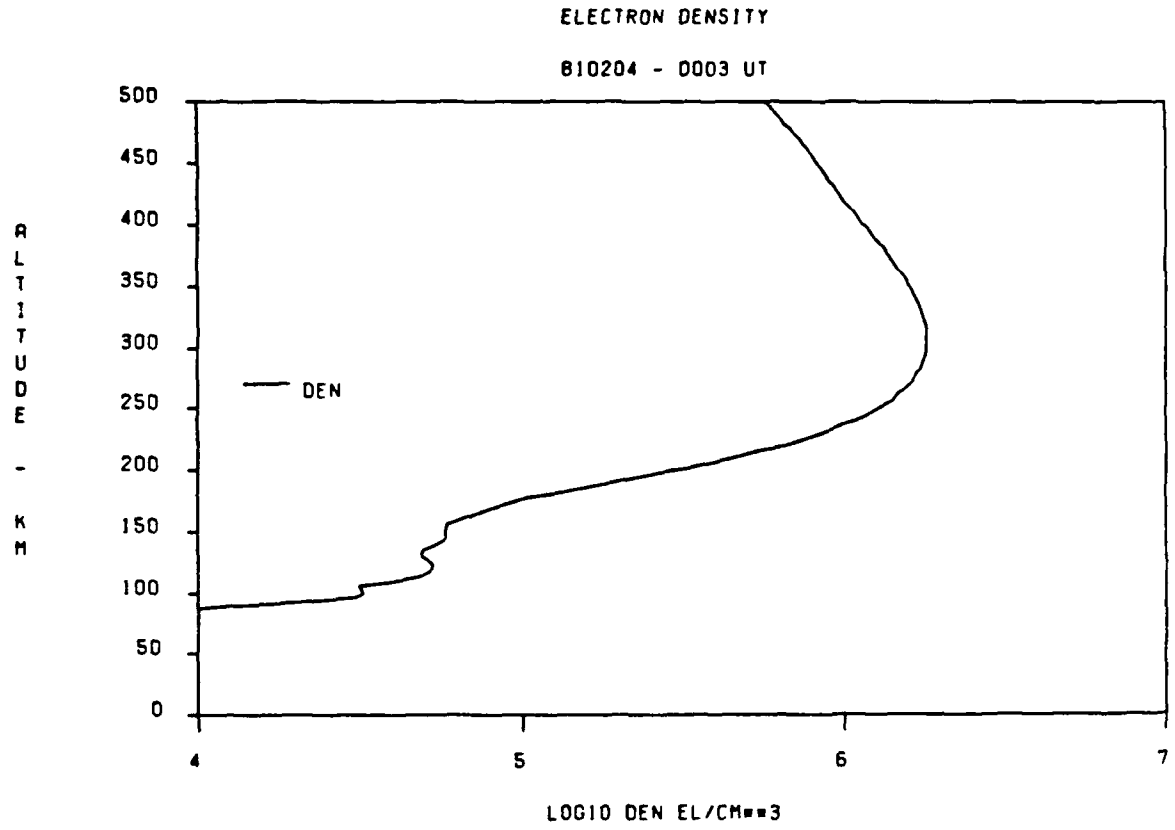
ELECTRON DENSITY
810204 - 0003 UT
500
450
400
350
300
250
200
150
100
50
0
ALTITUDE - KM
DEN
4
5
6
7
LOG10 DEN EL/CM**3

Fig. 8

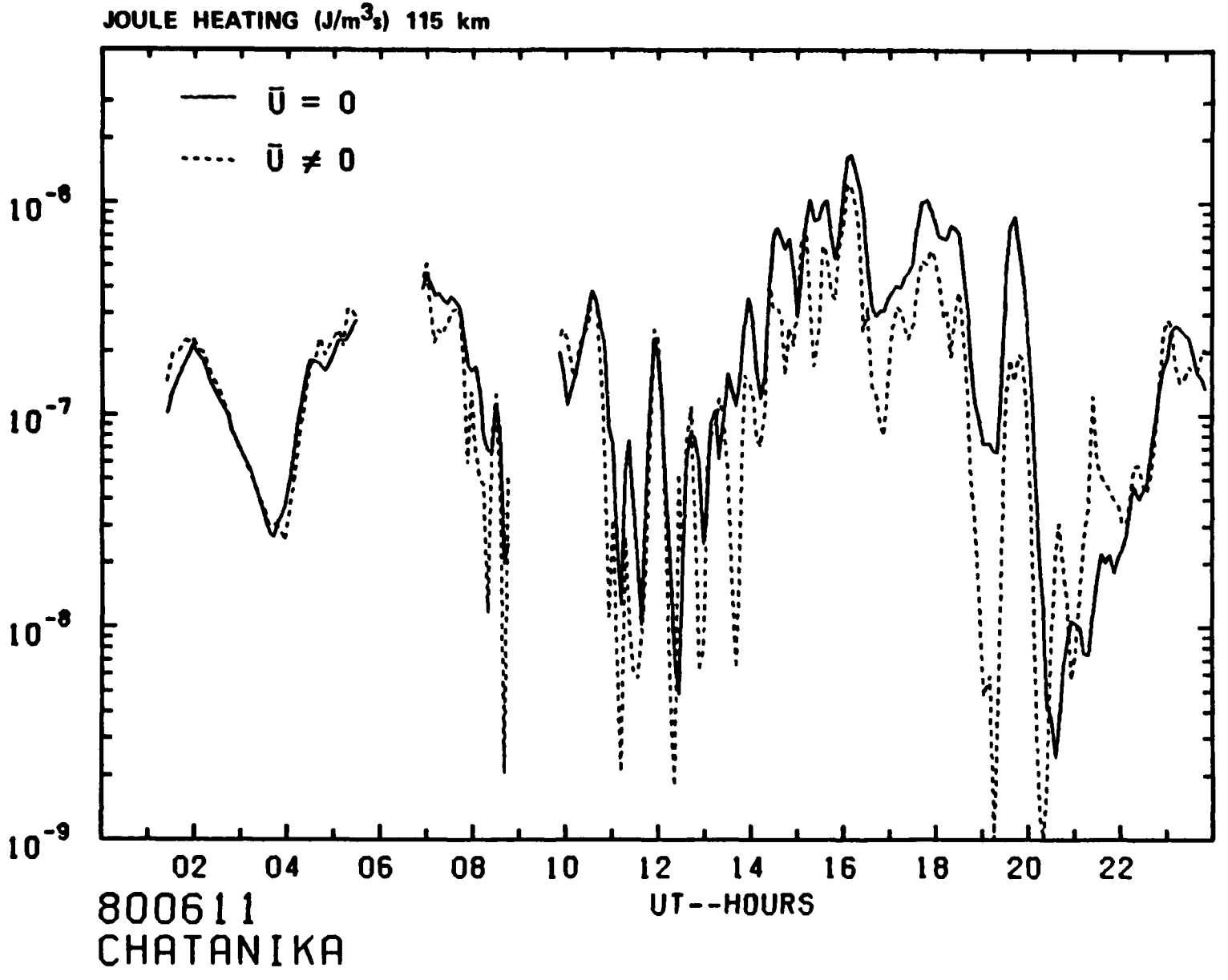

FIGURE 9. JOULE HEATING RATES AT 115 KM CALCULATED FOR CHATANIKA DATA ON 800611 NEGLECTING (solid curve) AND INCLUDING (dashed curve) THE EFFECT OF THE NEUTRAL WIND.